© 2017. Published by The Company of Biologists Ltd | Development (2017) 144, 4522-4529 doi:10.1242/dev.153262

STEM CELLS AND REGENERATION

RESEARCH REPORT

Co-expression of Tbx6 and Sox2 identifies a novel transient neuromesoderm progenitor cell state

Alok Javali[1,2,*], Aritra Misra[1,3,*], Karolis Leonavicius[4,5], Debalina Acharyya[1], Bhakti Vyas[1,3] and Ramkumar Sambasivan[1,‡]

ABSTRACT

Elongation of the body axis is a key aspect of body plan development. Bipotential neuromesoderm progenitors (NMPs) ensure axial growth of embryos by contributing both to the spinal cord and mesoderm. The current model for the mechanism controlling NMP deployment invokes Tbx6, a T-box factor, to drive mesoderm differentiation of NMPs. Here, we identify a new population of Tbx6$^+$ cells in a subdomain of the NMP niche in mouse embryos. Based on co-expression of a progenitor marker, Sox2, we identify this population as representing a transient cell state in the mesoderm-fated NMP lineage. Genetic lineage tracing confirms the presence of the *Tbx6*$^+$ NMP cell state. Furthermore, we report a novel aspect of the documented *Tbx6* mutant phenotype, namely an increase from two to four ectopic neural tubes, corresponding to the switch in NMP niche, thus highlighting the importance of *Tbx6* function in NMP fate decision. This study emphasizes the function of Tbx6 as a bistable switch that turns mesoderm fate 'on' and progenitor state 'off', and thus has implications for the molecular mechanism driving NMP fate choice.

KEY WORDS: Neuromesoderm progenitors, Tbx6, Axial elongation, Trunk-tail transition, Mouse

INTRODUCTION

The discovery of neuromesoderm progenitors (NMPs) has fundamentally impacted our understanding of the development of vertebrate body plan (Henrique et al., 2015; Stern et al., 2006; Steventon and Martinez Arias, 2017). NMPs constitute a distinct population of stem cells that allow axial growth of vertebrate embryos by contributing to the posterior spinal cord (neural tube) and the somite-forming paraxial mesoderm. In particular, clonal lineage analysis has revealed that NMPs include bipotent stem cells capable of generating either neural or mesodermal progenitors (Martin and Kimelman, 2012; Tzouanacou et al., 2009). In the progenitor state, NMPs are marked by co-expression of the mesoderm T-box transcription factor brachyury (T) and the progenitor/neural marker Sox2 (Cambray and Wilson, 2007; Delfino-Machin et al., 2005; Garriock et al., 2015; Martin and Kimelman, 2012; Wilson et al., 2009). The feedback loop involving Wnt/β-catenin signaling and its target T is speculated to be key for maintenance of the NMP pool (Martin and Kimelman, 2012). By contrast, another T-box factor, Tbx6, a downstream target of T, is implicated in favoring the mesodermal aspect of the binary fate choice. *Tbx6* is required for repression of *Sox2* (Takemoto et al., 2011; Nowotschin et al., 2012; Bouldin et al., 2015; Ruvinsky et al., 1998). Moreover, a negative feedback of *Tbx6* on *Wnt3a* may favor exit of NMPs from the undifferentiated progenitor state (Martin and Kimelman, 2012). Based on this evidence, Tbx6 has been proposed as a fate switch, tipping the balance between NMP and mesoderm towards the latter. The fate switch function would predict induction of Tbx6 in the progenitor state; however, Tbx6 has been detected only in the differentiated paraxial mesoderm and not in progenitors. This missing evidence leaves a gap in our understanding of the timing of NMP fate restriction.

Local signaling cues are central to fate determination of stem cell descendants and hence the anatomy of the niche is crucial. In mouse, fate mapping studies have located NMPs in the node-primitive streak border (NSB) and caudal lateral epiblast (CLE) in late gastrula embryos and in the chordo-neural hinge (CNH) in tail bud stage embryos (Cambray and Wilson, 2002, 2007; Delfino-Machin et al., 2005; Martin and Kimelman, 2012). The NMPs in the NSB and CLE contribute to axial growth of the interlimb (trunk) region. A recent study has refined the CLE fate map by showing that bipotent trunk NMPs are restricted to anterior CLE, i.e. near the node, and that other subdomains of the CLE predominantly harbor cells with neuromesoderm potency, but with their fate restricted to either the neural or mesodermal lineage (Wymeersch et al., 2016). This implies discrete microenvironments within the CLE that favor maintenance or lineage progression of NMPs. Nevertheless, owing to an absence of markers for distinct subpopulations, molecular evidence for discrete subdomains of the niche is lacking.

As trunk development ends, NMPs from the NSB/CLE are relocated to the CNH of the tail bud (Cambray and Wilson, 2002, 2007; Wymeersch et al., 2016). The CNH is the region abutting the posterior end of the notochord ventral to the developing neural tube. NMPs in the CNH continue to contribute to neural tube and mesoderm in the tail. Tail bud-mediated tail development represents a mode of axial growth distinct from that of gastrulation-driven development of the trunk (reviewed by Handrigan, 2003). The axial level of the hindlimb buds marks the trunk-to-tail developmental transition. Strikingly, the mechanism governing the trunk-to-tail transition also appears to regulate the relocation of NMPs, thereby underscoring a mechanistic coupling of the switch in the NMP niche and this important developmental transition (Jurberg et al., 2013). However, the role of the key regulators of NMP fate in this key aspect of their biology remains unexplored.

Here, we show co-expression of Tbx6 and Sox2 in the primitive streak/CLE region. Later in development, in the tail bud, we find

[1]Institute for Stem Cell Biology and Regenerative Medicine, GKVK Campus, Bellary Road, Bengaluru 560065, India. [2]National Centre for Biological Sciences, TIFR, GKVK Campus, Bellary Road, Bengaluru 560065, India. [3]Manipal University, Madhav Nagar, Manipal 576104, India. [4]Life Science Research Center, Vilnius University, Saulėtekio al. 7, LT10223 Vilnius, Lithuania. [5]Department of Physiology Anatomy and Genetics, Oxford University, Le Gros Clark Building, South Parks Road, Oxford OX1 3QX, UK.
*These authors contributed equally to this work

‡Author for correspondence (ramkumars@instem.res.in)

D.A., 0000-0002-4692-6111; R.S., 0000-0001-8158-4367

Received 10 April 2017; Accepted 20 October 2017

Development (2017) 144, 4522-4529 doi:10.1242/dev.153262

Tbx6$^+$ Sox2$^+$ NMPs in the CNH. The distribution in the progenitor compartment as well as the co-expression with a progenitor marker indicate that these Tbx6$^+$ cells represent a transient progenitor population intermediate in the NMP lineage between the stem cells and the descendant mesoderm. Furthermore, our analysis of *Tbx6* mutants reveals a novel aspect of the NMP developmental phenotype coincident with the relocation of the NMP niche during the trunk-to-tail developmental transition. In summary, the study reveals a new Tbx6$^+$ Sox2$^+$ transition state in the NMP lineage and underscores the pivotal function of *Tbx6* in these developmentally important stem cells. These findings also provide key missing evidence supporting the current model of NMP fate choice and emphasize the role of Tbx6 as a switch that drives NMPs to adopt mesoderm fate.

RESULTS AND DISCUSSION

Tbx6/Sox2 co-expression identifies a new population of mesoderm-primed trunk NMPs

Tbx6 is proposed to be the decisive factor favoring exit of NMPs from the progenitor state toward mesoderm differentiation. The model predicts that Tbx6 expression should precede NMP fate commitment to paraxial mesoderm. However, evidence for this is scant from documented *Tbx6* expression (Garriock et al., 2015; Nowotschin et al., 2012). To test the prediction of the model we assayed for Tbx6 expression in the trunk NMP compartment using a custom-made Tbx6 antibody. Following antibody specificity confirmation (Fig. S1), we performed immunostaining of cryosections from wild-type E8.5 mouse embryos. Transverse series were stained for Tbx6 and Sox2. In addition to paraxial mesoderm, Tbx6$^+$ cells were observed in the region encompassing the primitive streak and CLE (Fig. 1A). Remarkably, these cells co-expressed Sox2 (Fig. 1A). To assess the distribution of Tbx6$^+$ Sox2$^+$ cells in primitive streak versus CLE, adjacent sections of the series were stained for T and fibronectin 1 (Fn1), a marker of the extracellular matrix (ECM). Whereas CLE is bounded ventrally by unbroken ECM, primitive streak has discontinuous ECM, characteristic of epithelial-to-mesenchymal transition. The results show that the majority of double-positive cells are present in the primitive streak, with some present in the medial aspect of the CLE as well (Fig. 1A). However, Tbx6 could not be detected unambiguously in the NSB and in epithelium corresponding to the anterior one-fifth of the CLE (Fig. 1A), where the uncommitted bipotent progenitors reside (Wymeersch et al., 2016). This appears consistent with previous single-cell analysis indicating the absence of *Tbx6* RNA in NMPs at E8.5 (Gouti et al., 2017; Koch et al., 2017).

For quantitative analysis, we focused on the posterior part of the CLE expressing Tbx6 in whole-mount immunostained E8.5 mouse embryos. All confocal optical sections passing through the posterior part of the CLE and primitive streak were analyzed. As spatial references, we used the posterior tip of the epiblast and a midline running along the primitive streak. Consistent with the above data, Tbx6$^+$ Sox2$^+$ cells were distributed near the midline of the primitive streak/CLE zone (Fig. 1B,C, Fig. S2). Noticeably, Tbx6$^+$ cells dwindled caudorostrally within this zone (Fig. 1C, Table S1). These results locate the majority of Tbx6$^+$ Sox2$^+$ cells in the midline, which has no neuromesoderm potency (Cambray and Wilson, 2007). A proportion of double-positive cells were distributed in the posterior part of the CLE, a region documented to possess some neuromesoderm potency, but predominantly mesoderm-fated progenitors (Cambray and Wilson, 2007; Wymeersch et al., 2016). Nearly one-third of the progenitors in the analyzed region were Tbx6$^+$ Sox2$^+$ (Fig. 1C, Table S1), with the level of Tbx6 lower than that in presomitic mesoderm (Fig. 1C). Based on the anatomical distribution and co-expression with Sox2, we conclude that the Tbx6$^+$ cells represent a mesoderm-primed transient progenitor state of trunk NMPs.

These experiments are the first to formally test the prediction of a Tbx6$^+$ Sox2$^+$ transient state and provide strong support for the model ascribing a decisive role for Tbx6 in the mesodermal fate of NMPs. Further, we suggest that the low levels of Tbx6 in the transient state might function to inhibit neurogenesis via Sox2 suppression but may not be sufficient to activate paraxial mesoderm genes. Interestingly, suppressing *Sox2* in *Tbx6* mutants rescues ectopic neural tube formation yet fails to rescue paraxial mesoderm development (Takemoto et al., 2011). This points to a mechanistic uncoupling of *Tbx6* function in neural inhibition and transactivation of paraxial mesoderm genes such as *Msgn1* (Wittler et al., 2007; Chalamalasetty et al., 2014). Investigation of *Msgn1* induction in these cell compartments could shed light on the possible biphasic function of Tbx6 in the NMP lineage.

Tbx6/Sox2 co-expression marks NMPs in the tail bud

As gastrulation ends, the continued axial growth is assured by NMPs that translocate from the NSB/CLE to the CNH in the tail bud. To assess whether the progenitor compartment in the tail bud also expresses Tbx6, we performed immunostaining on E9.5 tail bud sagittal cryosections for Tbx6 and Sox2. We found Tbx6$^+$ Sox2$^+$ cells in the CNH, the region documented to harbor NMPs (Fig. 2). Co-expression of T and Tbx6 in this compartment, in adjacent sections, attests to Tbx6 expression in NMPs (Fig. 2). These results confirm Tbx6 induction prior to mesoderm differentiation in this NMP lineage. The difference in Tbx6 expression in the trunk versus tail NMP compartments might reflect differences in the signaling environment in the epiblast versus the tail bud niche. Thus, our findings suggest that the regulatory state of tail NMPs is different from that of trunk NMPs. This conclusion is consistent with the findings of a single-cell transcriptome study (Gouti et al., 2017), which reported distinct gene expression patterns in E8.5 and E9.5 NMPs.

Tbx6 lineage tracing marks the posterior neural tube

Given the co-expression with Sox2 in tail bud NMP progenitor compartment, we asked whether Tbx6$^+$ cells have neural differentiation potential. We generated a novel transgenic *Tbx6-Cre* mouse line for Cre-lox genetic tracing. First, we verified that the reporter matches the mesoderm expression of endogenous *Tbx6* (supplementary Materials and Methods, Figs S3, S4). To test whether the *Tbx6* lineage marks the posterior neural tube in addition to mesoderm, we analyzed transverse sections of *Tbx6-Cre:ROSA^{tdTom}* E10.5 embryos for tdTomato reporter expression at different levels on the anteroposterior axis. At the hindlimb level and in the tail, virtually the entire neural tube appeared to be *Tbx6-Tomato*$^+$ (Fig. 3A, Fig. S4), strongly supporting Tbx6 expression in tail bud NMPs. However, unexpectedly, the contribution begins at the level of cervical somites and the extent of contribution gradually increases in the interlimb neural tube (Fig. 3A), indicating *Tbx6-Cre* induction in trunk NMPs. Our analysis also revealed a contribution of *Tbx6* reporter-positive cells to a number of tissues including posterior neural crest (Fig. S4) (Concepcion et al., 2017).

Tbx6 lineage reporter expression in the neural tube at cervical and interlimb level appears discordant with undetectable Tbx6 in the NSB and anterior CLE (Fig. 1A) (Gouti et al., 2017). Therefore, we assessed *Tbx6* reporter expression in the CLE in E8.5 *Tbx6-Cre:ROSA^{tdTom}* embryos. The entire transverse section of the CLE,

Development (2017) 144, 4522-4529 doi:10.1242/dev.153262

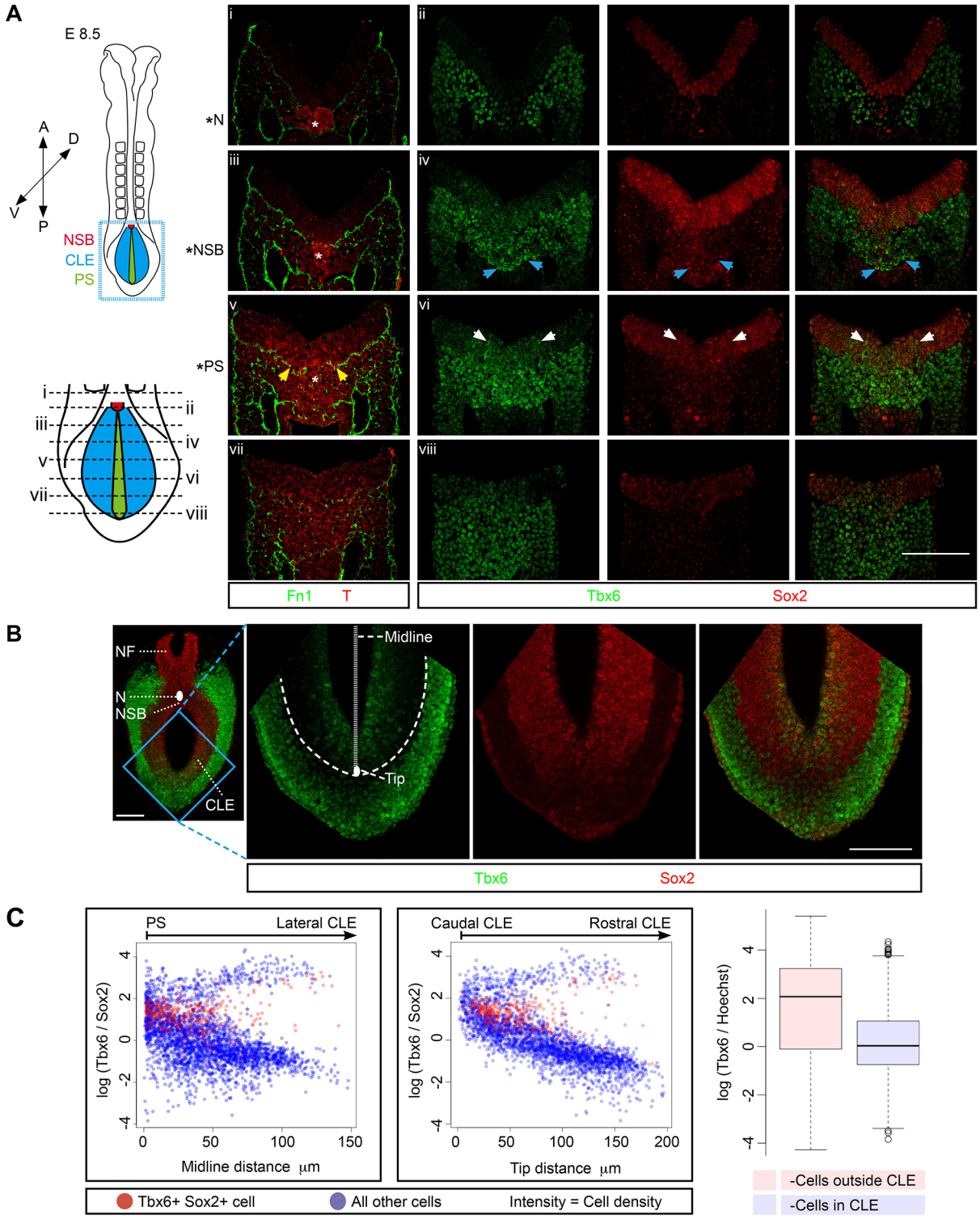

Fig. 1. See next page for legend.

including the T^+ $Sox2^+$ pool, was reporter positive (Fig. 3B). To address this discordance in *Tbx6* and reporter expression, we compared the expression of *Cre* RNA with that of endogenous *Tbx6*. We observed *Cre* expression in the NSB, while *Tbx6* RNA was unambiguously detected only in primitive streak posterior to the NSB (Fig. S5). In addition, we tested whether Tbx6 is induced in the NMP compartment earlier than E8.5, which could also explain the wider expression of reporter in NMP derivatives observed. As documented, we detected rare $Tbx6^+$ $Sox2^+$ cells in the NSB at E7.5 (Fig. S6) (Hadjantonakis et al., 2008). Taken together, transient induction of *Tbx6* in the NSB at E7.5 combined with expression of *Cre* transgene earlier in the lineage might account for reporter expression in the entirety of NMP derivatives. However, Tbx6 expression in the tail bud NMPs is independently corroborated by our analysis of the knock-in $Tbx6^{H2B\text{-}EYFP}$ [$Tbx6^{YFP}$ (Hadjantonakis et al., 2008)] reporter mouse line, which acts as a short-term tracer.

Development (2017) 144, 4522-4529 doi:10.1242/dev.153262

Fig. 1. Tbx6 and Sox2 co-expression marks a new transient progenitor state of the neuromesoderm lineage. (A) (Left) Illustration of NMP anatomy in an E8.5 mouse embryo. A, anterior; P, posterior; D, dorsal; V, ventral; NSB, node-primitive streak border; CLE, caudal lateral epiblast; PS, primitive streak. Box indicates the area shown in B. (Right) Transverse series (at the levels indicated bottom left) of cryosections co-immunostained for Fn1 and brachyury (T) or for Tbx6 and Sox2. Blue arrows mark ingressed cells; yellow arrows delimit discontinuous ECM and thus primitive streak; white arrows mark Tbx6$^+$ Sox2$^+$ cells in the CLE. Asterisks mark the node (N), NSB or PS. (B) Single confocal optical section at a dorsal level of immunostained whole-mount embryos. NF, neural folds. The midline of the primitive streak and the caudal tip of the primitive streak/CLE zone are indicated; these were used as geographical references for measurements performed in C. The gaps in the sections reflect invaginations in the neural plate (top; seen in the low-magnification image) and in the primitive steak (bottom). (C) Quantitative image analysis (from Embryo 1, see Table S1) of Tbx6 and Sox2 expression. The dots in the scatter plot represent cells in the geometrically defined CLE region and primitive streak. Fluorescence is represented by the logarithm of intensity normalized to Hoechst intensity. The dots represent the ratio of Tbx6 to Sox2 fluorescence, i.e. (Tbx6/Hoechst)/(Sox2/Hoechst). The dots are semi-transparent so that overlap of multiple dots is indicated by higher intensity. The box plot shows low levels of Tbx6 in the CLE compared with paraxial mesoderm (outside the CLE). The difference between the means in the two groups is fourfold; P=2.2×10^{-16} for the pairwise comparison. n=3 embryos. Scale bars: 100 µm.

We found strong and abundant YFP expression in the Sox2$^+$ posterior neural tube (Fig. 3C). Taking this result together with *Tbx6-Cre* tracing, we conclude that the *Tbx6* locus is 'open' in the NMP lineage much earlier than anticipated.

Understanding the regulatory cell state of stem cells is essential to deciphering the mechanisms controlling their maintenance and function. NMPs could either be a lineage non-committed 'naïve' population or a committed pool equipoised to both the neural and mesodermal lineages. NMPs have been proposed to represent the latter (Steventon and Martinez Arias, 2017) based on the co-expression of promesodermal T and proneural Sox2 factors. Transient induction of the *Tbx6* locus or its 'open' state does not equate to the presence of functional protein in trunk NMPs, but reflects a poised regulatory state. Furthermore, we suggest that mere induction of *Tbx6* alone might not be sufficient to effect a fate switch and that a threshold level might be required, at least in the tail. This idea is in accordance with the apparent difference in Tbx6 levels between the CNH and tail bud mesenchyme (Fig. 2).

Increased ectopic neural tubes in *Tbx6* null embryos at the trunk-tail transition correlates with NMP niche relocation

Since Tbx6 is expressed in NMPs of the CNH and virtually all cells in the tail are *Tbx6* lineage reporter positive, we wondered whether *Tbx6* loss of function would impact tail development more severely. In fact, a bulged tail bud with multiple ectopic neural rosettes in *Tbx6* mutants (Chapman and Papaioannou, 1998) hints at increasing phenotypic severity in the tail. We revisited the analysis of *Tbx6* mutant tail phenotype. No overt posterior neural tube patterning defect was observed (Fig. S7); however, strikingly, we found an increased number of ectopic neural tubes along the anteroposterior axis. By analyzing a series of transverse sections in E10.5 *Tbx6*$^{YFP/YFP}$ mutant embryos, we found a switch from two ectopic tubes at the base of the forelimb bud to four ectopic tubes at the axial level in register with the top of the hindlimb bud (Fig. 4A, Fig. S7). This phenotypic switch correlates with the transition from trunk to tail development, which entails reallocation of NMPs from the NSB/CLE to the CNH in the tail bud.

A priori, the supernumerary neural tubes could be due to expansion of the neurogenic progenitor domain. In fact, a broader domain of Sox2$^+$ neural progenitors in *Tbx6* mutant tail bud has been documented (Nowotschin et al., 2012). First, we ruled out the

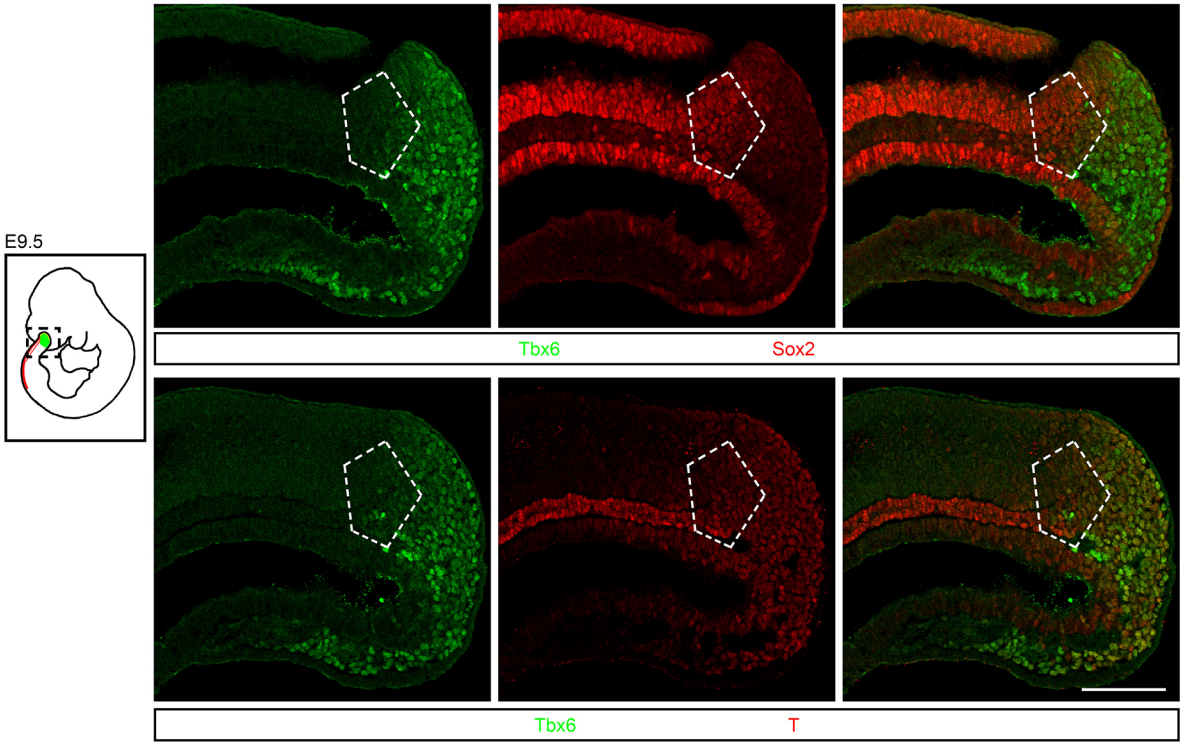

Fig. 2. Tail bud NMPs co-express Tbx6 and Sox2. (Top) Immunostaining of sagittal sections shows co-expression of Tbx6 and Sox2 in the CNH (pentagon). (Bottom) Adjacent section stained for the mesoderm marker T and Tbx6. n=3 embryos. Scale bar: 100 µm.

Development (2017) 144, 4522-4529 doi:10.1242/dev.153262

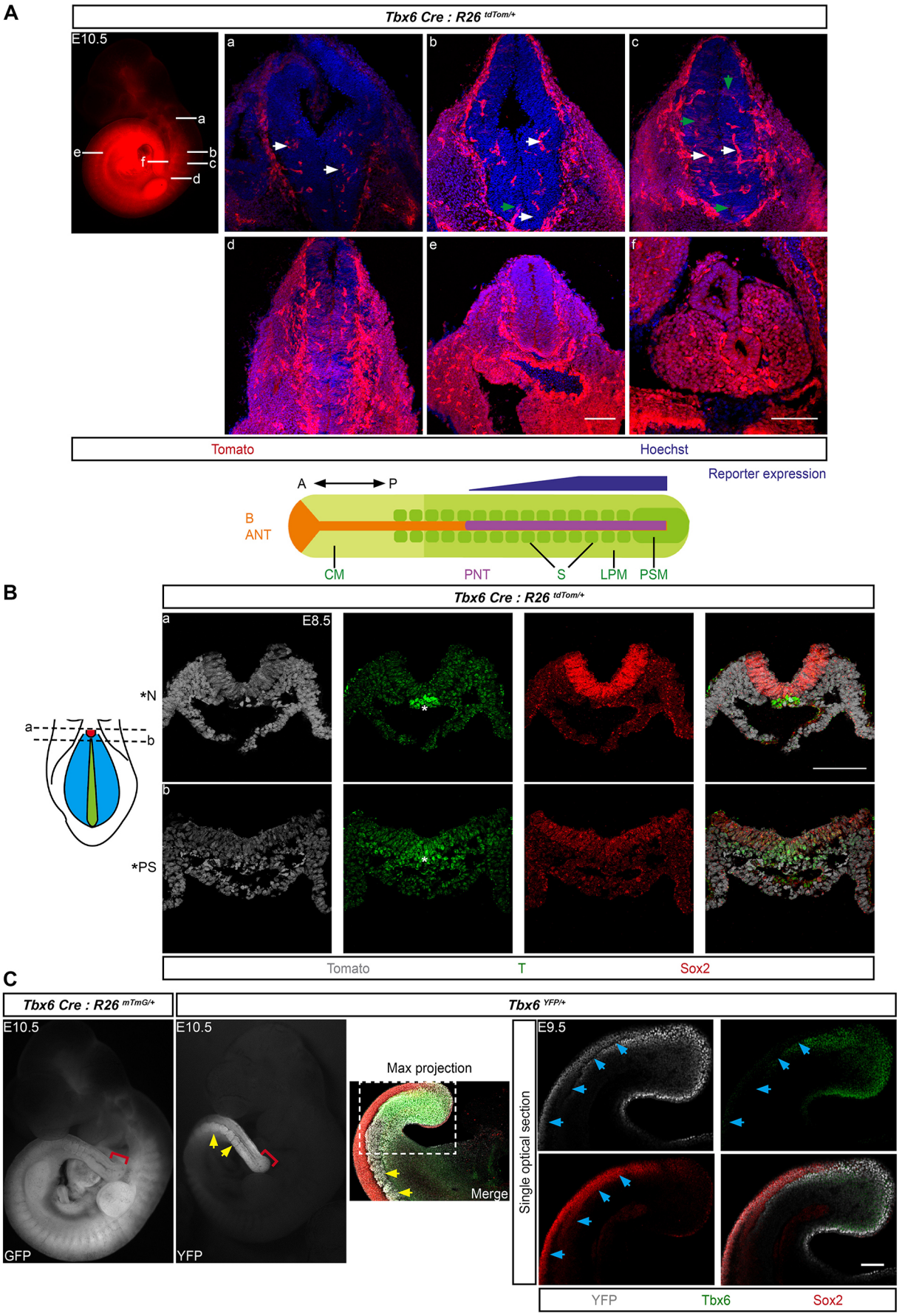

Fig. 3. See next page for legend.

Development (2017) 144, 4522-4529 doi:10.1242/dev.153262

Fig. 3. *Tbx6* lineage reporter marks virtually all NMP derivatives. (A) Live tdTomato reporter expression in a whole-mount embryo; the axial level of the transverse sections (a-f) is indicated. White arrows, endothelial cells (see Fig. S4); green arrows, neuroepithelial progenitors. The schematic beneath illustrates the findings. Blue gradient highlights the increase in reporter expression along the anteroposterior axis. A, anterior; P, posterior; B, brain; ANT, anterior neural tube; PNT, posterior neural tube; CM, cranial mesoderm; S, somites; LPM, lateral plate mesoderm; PSM, presomitic mesoderm. (B) Immunostained transverse cryosections (at levels a, b) show *Tbx6* reporter expression throughout the entire epithelium of the CLE fully overlapping the T^+ $Sox2^+$ zone. Asterisks indicate the node (N) or primitive streak (PS). (C) Comparison of the *Tbx6-Cre* reporter and the $Tbx6^{YFP}$ knock-in reporter shows the short-term tracing potential of the latter. The red bracket flags the domain of endogenous Tbx6 protein expression (see Fig. S1). Yellow arrows show the chase of *Tbx6* expression by YFP reporter in the somites. Sagittal confocal optical sections of the tail bud show $Tbx6^{YFP}$ reporter expression in $Sox2^+$ neural tube (blue arrows). *n*=3 embryos. Scale bars: 100 µm.

unlikely possibility that lateral plate mesoderm fate transformation contributes to the additional ectopic tubes (Fig. S7). Then, to directly assess whether the majority of the tail bud mesenchyme acquires neural fate, we analyzed the tail bud of $Tbx6^{YFP}$ heterozygotes and null mutants by immunostaining. Exploiting the *YFP* reporter, we found that 74.7±1.4% (*n*=4 embryos; total 4024 nuclei) overlap in YFP and Sox2 expression in mutants, as opposed to a more restricted co-expression of 28.3±2.9% (*n*=4 embryos; total 3213 nuclei) in the CNH region of heterozygotes (Fig. 4B). Based on these data we suggest that *Tbx6* function is required to restrict the neurogenic NMP pool to the CNH region.

In essence, defining the axial level at which the phenotypic transition occurs reveals an important link between *Tbx6* function and NMP behavior. The increase from two to four neural tubes appears to correspond to the change in NMP niche. Although conclusive demonstration is awaited, relocation from the CLE to CNH might involve a transition of NMPs from epithelium to mesenchyme. We suggest that the expansion of the neurogenic progenitor zone in mutants, together with the differences in the morphogenetic processes consequent to the epithelial-to-mesenchymal switch in the NMP niche, might explain the difference in the phenotype at the trunk and tail axial levels.

In summary, our findings establish the presence of a $Tbx6^+$ $Sox2^+$ transient progenitor population intermediate in the differentiation

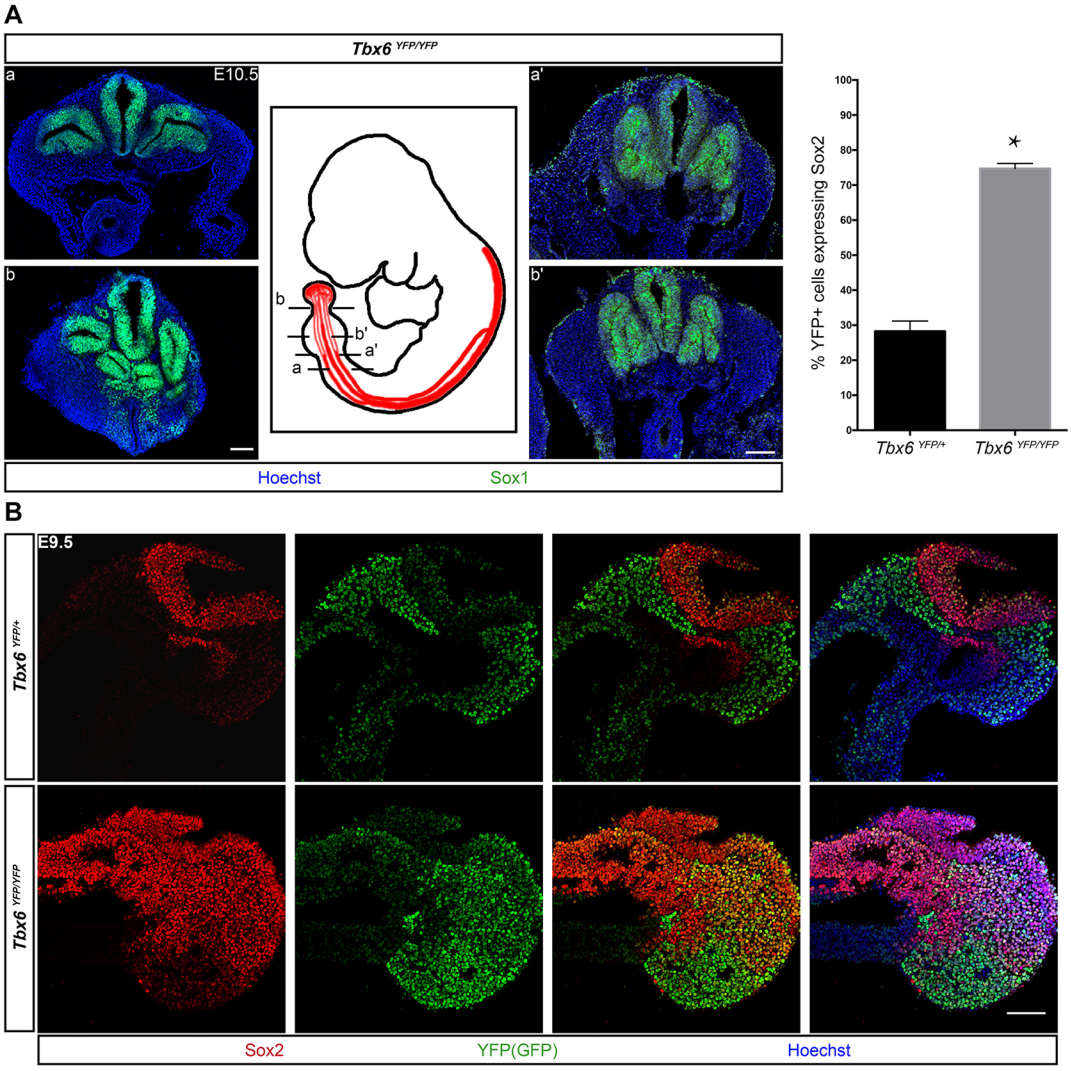

Fig. 4. Increase in ectopic neural tubes in the *Tbx6* mutant correlates with NMP niche relocation. (A) Immunostained cryosections (at levels a-b′) show four ectopic neural tubes in the tail bud (b). The switch from two to four ectopic neural tubes begins at the anterior end of hindlimb bud. *n*=6 embryos. (B) Sagittal sections of tail bud stained for YFP (antibody against GFP) and Sox2. Bar chart shows quantification of the increased proportion of $Sox2^+$ cells expressing YFP. *n*=3 embryos. Mann–Whitney test, two-tailed; error bars are s.e.m.; **P*=0.0286. Scale bars: 100 µm.

Development (2017) 144, 4522-4529 doi:10.1242/dev.153262

of NMP stem cells into paraxial mesoderm. This proof of Tbx6 expression marking the transition cell state strongly supports the current model of NMP fate decisions and emphasizes the role of Tbx6 as a fate switch or a 'fate dial' controlling mesoderm differentiation. These findings, along with the graded *Tbx6* mutant phenotype during the trunk to tail transition coincident with NMP niche relocation, underscore the central role of Tbx6 in NMP biology. Broadly, NMPs are crucial to the construction of the vertebrate body plan and our findings have a bearing on understanding the biology of this important pool of developmental stem cells.

MATERIALS AND METHODS

Mouse strains

All experiments on mice were carried out in compliance with Committee for the Purpose of Control and Supervision of Experiments on Animals (CPCSEA) national guidelines. All experimental procedures were approved by the inStem Institutional Animal Ethics Committee. Strains used: $Tbx6^{YFP/+}$ (Hadjantonakis et al., 2008), *Tbx6-Cre* (see supplementary Materials and Methods), $R26^{mTmG/+}$ (Muzumdar et al., 2007), $R26^{tdTom/+}$ (Madisen et al., 2010) and $R26^{nlacZ/+}$ (Tzouanacou et al., 2009).

Immunostaining

For whole-mount immunostaining, embryos were fixed in 4% paraformaldehyde (PFA) in PBS for 90 min at 4°C. Embryos were blocked from non-specific antibody binding in blocking solution containing 0.5% Triton X-100 and 10% normal donkey serum. The embryos were treated overnight at 4°C with primary antibodies diluted in the blocking solution, followed by 1 h incubation in PBS containing 0.1% Tween 20, 10 mg/ml Hoechst and 4 mg/ml secondary antibodies.

For cryosections, embryos were embedded in PBS containing 7% gelatin and 15% sucrose following fixation in 4% PFA in PBS for 90-120 min and cryoprotection by equilibration in 15% sucrose in PBS overnight. The embryos were sectioned at 16 µm thickness using a Leica CM 1850 UV cryostat. Select sections were stained as described for whole-mount immunostaining.

For immunostaining cultured cells, the cells were fixed with 4% PFA for 15 min at ambient temperature and permeabilized using 0.3% Triton X-100 in PBS for 30 min and further blocked in PBS with 0.3% Triton X-100 and 5% normal donkey serum for 1 h. Incubation with primary antibody in blocking solution was carried out overnight at 4°C. The secondary antibody treatment was performed as described for whole-mount immunostaining.

Polyclonal anti-Tbx6 antibody used in this study was raised in rabbit against mouse Tbx6 using a peptide immunogen of the following sequence CFHGAPSHLPARTPSFAEAPDPGRPAPYS and affinity purified (Imgenex India). The specificity of the antibody has been tested by immunostaining as well as in immunoblot assays (Fig. S1). Images were acquired using a confocal or inverted fluorescence microscope. See the supplementary Materials and Methods for details and Table S2 for information about the antibodies used.

Quantitative image analysis

Images were analyzed using a probabilistic approach, which relies on nuclear segmentation using a Hough transform-based voting algorithm to detect cell positions in space, followed by pixel classification using the nuclear marker. The image analysis platform 'SilentMark' (Leonavicius et al., 2017 preprint) is available as an online data analysis application provided by Droplet Genomics (http://data.dropletgenomics.com/new/experiment/SilentMark). See the supplementary Materials and Methods for details.

In situ RNA hybridization

Whole-mount RNA *in situ* hybridization was performed following an established protocol (Henrique et al., 1995). The incubation period for proteinase K treatment was empirically determined for different stages of the mouse embryos. To detect *Dermo1*, a probe against its 3′ UTR was used, while *Tbx6* and *Cre* probes were prepared against the coding sequences. The antisense riboprobes were generated by *in vitro* transcription incorporating Digoxigenin-11_UTP (Roche). Washes following the incubation with alkaline phosphatase (AP)-conjugated anti-Digoxigenin-11 antibodies were extended for 48 h and BM Purple (Roche) was used as the colorigenic substrate for AP.

X-gal staining

Embryos were fixed for 40 min to 1 h in 4% PFA, washed in PBS and stained overnight at room temperature in a standard X-gal staining solution (Sanes et al., 1986).

Acknowledgements

We thank the animal facility (ACRC-NCBS/inStem), Central Imaging & Flow Cytometry Facility (NCBS) and Stem Cell Facility (inStem). We thank Prof. Virginia Papaioannou for the $Tbx6^{YFP}$ mouse strain; Prof. Shahragim Tajbhaksh and Dr Francina Langa-Vives for help in generating the *Tbx6-Cre* strain; Drs Moises Mallo and Akash Gulyani for discussion; and Prof. Jyotsna Dhawan and Dr Ben Steventon for critical reading of the manuscript.

Competing interests

The authors declare no competing or financial interests.

Author contributions

Conceptualization: A.J., A.M., R.S.; Methodology: A.J., A.M., K.L., D.A., B.V.; Software: K.L.; Validation: A.J., A.M., B.V.; Formal analysis: A.J., A.M., K.L., R.S.; Investigation: A.J., A.M., D.A., B.V.; Writing - original draft: R.S.; Writing - review & editing: A.J., A.M., K.L., R.S.; Visualization: A.J., A.M., K.L., D.A., B.V.; Supervision: R.S.; Project administration: R.S.; Funding acquisition: R.S.

Funding

A.J. receives a National Centre for Biological Sciences (NCBS)-Tata Institute of Fundamental Research (TIFR) PhD fellowship; A.M. and D.A. receive an inStem fellowship from the Department of Biotechnology, Ministry of Science and Technology, India (DBT); and B.V. is a DBT Junior Research Fellow. R.S. is a DBT-Ramalingaswami Fellow (BT/RLF/Re-entry/03/2010). The work is supported by DBT grants BT/PR13640/MED/97/263/2015, BT/PR12017/MED/31/282/2014 and inStem. Animal work was partially supported by DBT-NaMoR grant BT/PR5981/MED/31/181/2012.

Supplementary information

Supplementary information available online at
http://dev.biologists.org/lookup/doi/10.1242/dev.153262.supplemental

References

Bouldin, C. M., Manning, A. J., Peng, Y.-H., Farr, G. H., Hung, K. L., Dong, A. and Kimelman, D. (2015). Wnt signaling and tbx16 form a bistable switch to commit bipotential progenitors to mesoderm. *Development* **142**, 2499-2507.

Cambray, N. and Wilson, V. (2002). Axial progenitors with extensive potency are localised to the mouse chordoneural hinge. *Development* **129**, 4855-4866.

Cambray, N. and Wilson, V. (2007). Two distinct sources for a population of maturing axial progenitors. *Development* **134**, 2829-2840.

Chalamalasetty, R. B., Garriock, R. J., Dunty, W. C., Kennedy, M. W., Jailwala, P., Si, H. and Yamaguchi, T. P. (2014). Mesogenin 1 is a master regulator of paraxial presomitic mesoderm differentiation. *Development* **141**, 4285-4297.

Chapman, D. L. and Papaioannou, V. E. (1998). Three neural tubes in mouse embryos with mutations in the T-box gene Tbx6. *Nature* **391**, 695-697.

Concepcion, D., Washkowitz, A. J., Desantis, A., Ogea, P., Yang, J. I., Douglas, N. C. and Papaioannou, V. E. (2017). Cell lineage of timed cohorts of Tbx6-expressing cells in wild-type and Tbx6 mutant embryos. *Biol. Open* **6**, 1065-1073.

Delfino-Machin, M., Lunn, J. S., Breitkreuz, D. N., Akai, J. and Storey, K. G. (2005). Specification and maintenance of the spinal cord stem zone. *Development* **132**, 4273-4283.

Garriock, R. J., Chalamalasetty, R. B., Kennedy, M. W., Canizales, L. C., Lewandoski, M. and Yamaguchi, T. P. (2015). Lineage tracing of neuromesodermal progenitors reveals novel Wnt-dependent roles in trunk progenitor cell maintenance and differentiation. *Development* **142**, 1628-1638.

Gouti, M., Delile, J., Stamataki, D., Wymeersch, F. J., Huang, Y., Kleinjung, J., Wilson, V. and Briscoe, J. (2017). A gene regulatory network balances neural and mesoderm specification during vertebrate trunk development. *Dev. Cell* **41**, 243-261.

Hadjantonakis, A.-K., Pisano, E. and Papaioannou, V. E. (2008). Tbx6 regulates left/right patterning in mouse embryos through effects on nodal cilia and perinodal signaling. *PLoS ONE* **3**, e2511.

Handrigan, G. R. (2003). Concordia discors: duality in the origin of the vertebrate tail. *J. Anat.* **202**, 255-267.

Development (2017) 144, 4522-4529 doi:10.1242/dev.153262

Henrique, D., Adam, J., Myat, A., Chitnis, A., Lewis, J. and Ish-Horowicz, D. (1995). Expression of a Delta homologue in prospective neurons in the chick. *Nature* **375**, 787-790.

Henrique, D., Abranches, E., Verrier, L. and Storey, K. G. (2015). Neuromesodermal progenitors and the making of the spinal cord. *Development* **142**, 2864-2875.

Jurberg, A. D., Aires, R., Varela-Lasheras, I., Nóvoa, A. and Mallo, M. (2013). Switching axial progenitors from producing trunk to tail tissues in vertebrate embryos. *Dev. Cell* **25**, 451-462.

Koch, F., Scholze, M., Wittler, L., Schifferl, D., Sudheer, S., Grote, P., Timmermann, B., Macura, K. and Herrmann, B. G. (2017). Antagonistic activities of Sox2 and brachyury control the fate choice of neuro-mesodermal progenitors. *Dev. Cell* **42**, 514-526.

Leonavicius, K., Royer, C., Miranda, A. M. A., Tyser, R., Kip, A. and Srinivas, S. (2017). Spatial protein analysis in developing tissues: a sampling-based image processing approach. *BioRxiv* 163147.

Madisen, L., Zwingman, T. A., Sunkin, S. M., Oh, S. W., Zariwala, H. A., Gu, H., Ng, L. L., Palmiter, R. D., Hawrylycz, M. J., Jones, A. R. et al. (2010). A robust and high-throughput Cre reporting and characterization system for the whole mouse brain. *Nat. Neurosci.* **13**, 133-140.

Martin, L. B. and Kimelman, D. (2012). Canonical Wnt signaling dynamically controls multiple stem cell fate decisions during vertebrate body formation. *Dev. Cell* **22**, 223-232.

Muzumdar, M. D., Tasic, B., Miyamichi, K., Li, L. and Luo, L. (2007). A global double-fluorescent Cre reporter mouse. *Genesis* **45**, 593-605.

Nowotschin, S., Ferrer-Vaquer, A., Concepcion, D., Papaioannou, V. E. and Hadjantonakis, A.-K. (2012). Interaction of Wnt3a, Msgn1 and Tbx6 in neural versus paraxial mesoderm lineage commitment and paraxial mesoderm differentiation in the mouse embryo. *Dev. Biol.* **367**, 1-14.

Ruvinsky, I., Silver, L. M., Ho, R. K., We, A. and Xombi, X. (1998). Characterization of the zebrafish tbx16 gene and evolution of the vertebrate T-box family. *Dev. Genes Evol.* **208**, 94-99.

Sanes, J. R., Rubenstein, J. L. and Nicolas, J. F. (1986). Use of a recombinant retrovirus to study post-implantation cell lineage in mouse embryos *EMBO J.* **5**, 3133-3142.

Stern, C. D., Charité, J., Deschamps, J., Duboule, D., Durston, A. J., Kmita, M., Nicolas, J.-F., Palmeirim, I., Smith, J. C. and Wolpert, L. (2006). Head-tail patterning of the vertebrate embryo: one, two or many unresolved problems? *Int. J. Dev. Biol.* **50**, 3-15.

Steventon, B. and Martinez Arias, A. (2017). Evo-engineering and the cellular and molecular origins of the vertebrate spinal cord. *Dev. Biol.* **432**, 3-13.

Takemoto, T., Uchikawa, M., Yoshida, M., Bell, D. M., Lovell-Badge, R., Papaioannou, V. E. and Kondoh, H. (2011). Tbx6-dependent Sox2 regulation determines neural or mesodermal fate in axial stem cells. *Nature* **470**, 394-398.

Tzouanacou, E., Wegener, A., Wymeersch, F. J., Wilson, V. and Nicolas, J.-F. (2009). Redefining the progression of lineage segregations during mammalian embryogenesis by clonal analysis. *Dev. Cell* **17**, 365-376.

Wilson, V., Olivera-Martínez, I. and Storey, K. G. (2009). Stem cells, signals and vertebrate body axis extension. *Development* **136**, 2133-2133.

Wittler, L., Shin, E.-H., Grote, P., Kispert, A., Beckers, A., Gossler, A., Werber, M. and Herrmann, B. G. (2007). Expression of Msgn1 in the presomitic mesoderm is controlled by synergism of WNT signalling and Tbx6. *EMBO Rep.* **8**, 784-789.

Wymeersch, F. J., Huang, Y., Blin, G., Cambray, N., Wilkie, R., Wong, F. C. K. and Wilson, V. (2016). Position-dependent plasticity of distinct progenitor types in the primitive streak. *Elife* **5**, e10042.

Supplementary methods:

Mouse strains and generation of *Tbx6-Cre* mouse line

Mice were maintained on a 14 hours light / 10 hours dark cycle. For staging the embryos, the morning of vaginal plug detection was considered as E 0.5. Wildtype strain used for the experiments is C57BL/6J:DBA2-F1 hybrid.

The *Tbx6-Cre* line was created using a bacterial artificial chromosome (BAC) transgenic approach such that Cre recombinase is driven by *Tbx6* regulatory sequences (Figure S3). A bacterial artificial chromosome (BAC; clone# RP24 239G12 from CHORI, USA) containing *Tbx6* locus with approximately 84 Kb upstream, 4 Kb of the open reading frame and 73 Kb downstream sequences was chosen (Figure S1). The Cre recombinase expression cassette was engineered into this BAC at the 1st exon of *Tbx6* such that 14 nucleotides (25th to 39th bases) including the ATG are removed (See Figure S2). BAC recombineering were performed using GeneBridges Red/ET recombination system. The targeting cassette contained about 50 bp of 5' and 3' homology arms, a Cre recombinase encoding cDNA followed by bovine growth hormone poly A signal and a dual eukaryotic / prokaryotic selection cassette for Neomycin/Kanamycin resistance flanked by loxP sites. Following selection of the targeted BAC in E.coli using Kanamycin, the selection cassette was floxed out in bacteria by introducing a prokaryotic Cre expression vector. After verification of the recombination with primers (shown in Figure S2), the circular BAC engineered with Cre was microinjected into oocytes to generate transgenic strains. Four independent strains showed similar pattern of transgene expression as assessed by flox-reporter activation. As we did not find any apparent differences between these strains, we have performed all experiments presented here with only one of the strains. To assess whether the *Cre* transgene expression matches endogenous gene expression, we performed RNA *in situ* hybridization through a developmental time series relevant for *Tbx6* expression. As shown in Figure S3, the spatiotemporal patterns of *Cre* RNA and of *Tbx6* RNA match. *Tbx6* expression is detectable between E7 and E7.5 in mouse embryos and marks the mesoderm that ingress through the primitive streak (Chapman et al., 1996). As mesoderm develops further it continues to mark the paraxial component of the mesoderm until somite formation (Chapman et al., 1996; Windner et al., 2015; Yasuhiko et al., 2006). From embryonic day (E) 8.5, *Tbx6* is expressed in the tail bud (Chapman et al., 1996). Overall *Cre* RNA expression matches this pattern. When *Tbx6-Cre* were mated with *ROSA*^{mTmG} reporter lines, the *Tbx6-Cre:ROSA*^{mTmG} embryos revealed broad mesodermal expression of the reporter (Figure S3). To assess in detail the lineage of Tbx6+ cells, we generated *Tbx6-Cre:ROSA*^{nlacZ} embryos at E10.5, stained them with X-gal and analyzed cross-sections. These sections revealed strong reporter expression in the somites as well as in the lateral plate mesoderm (Figure S4).

Microscopy imaging and analysis

Imaging of X-gal and *in situ* hybridization stained embryos as well as that of whole embryos for live reporter expression was performed using Olympus SZX16 stereomicroscope with Olympus DP72 camera. The fluorescent images of immunostained section and whole mount embryos were acquired using Olympus fv1000 confocal microscope. The confocal images were analyzed and assembled using ImageJ.

Quantitative image analysis

Nuclear fluorescence was measured from a 3.2 μ radius region around the detected nuclear position using pixels classified as positive for the nuclear marker. Tissue geometry analysis was based on manually designated regions of interest, which were defined using Sox2 expression and anatomy as reference. Data representing nuclear fluorescence and distance from marked regions of interest was processed using RStudio (v.099), running R (v.3.3.3) for statistical testing and visualization. Fluorescence levels were internally normalized as a ratio to nuclear marker fluorescence (Hoechst), which compensates for changes in tissue opacity and imaging depth. Fluorescence level was then represented as a natural logarithm of the ratio for further statistical analyses. To identify cells positive for either Sox2 or Tbx6 nuclear markers, fluorescence levels were thresholded using distribution scatter plot (Fig. S2) and identifying two separate cell populations. Statistical significance between pairwise fluorescence level comparisons was tested using student's t-test and the corresponding p-value.

NMPs are restricted to NSB and the anterior 1/5th of CLE and the posterior 4/5th appear mesoderm-fated at 6-somite staged embryo (Wymeersch et al., 2016). We refer to CLE excluding the domain of uncommitted NMP as posterior part of CLE. We find that at 10-somite stage, the entire CLE region from NSB to posterior tip of CLE / primitive streak zone is encompassed in 5 – 6 cryosections of ~16 μm. Tbx6 is clearly detected only in the four posterior sections. The fate and potency maps may be different for the older embryos analyzed, however, here we assume it to be similar to that of 6-somite stage. Note, the diamond-shaped region imaged in wholemount embryos for quantitative analysis covers majority of this posterior part of CLE.

Supplementary figures

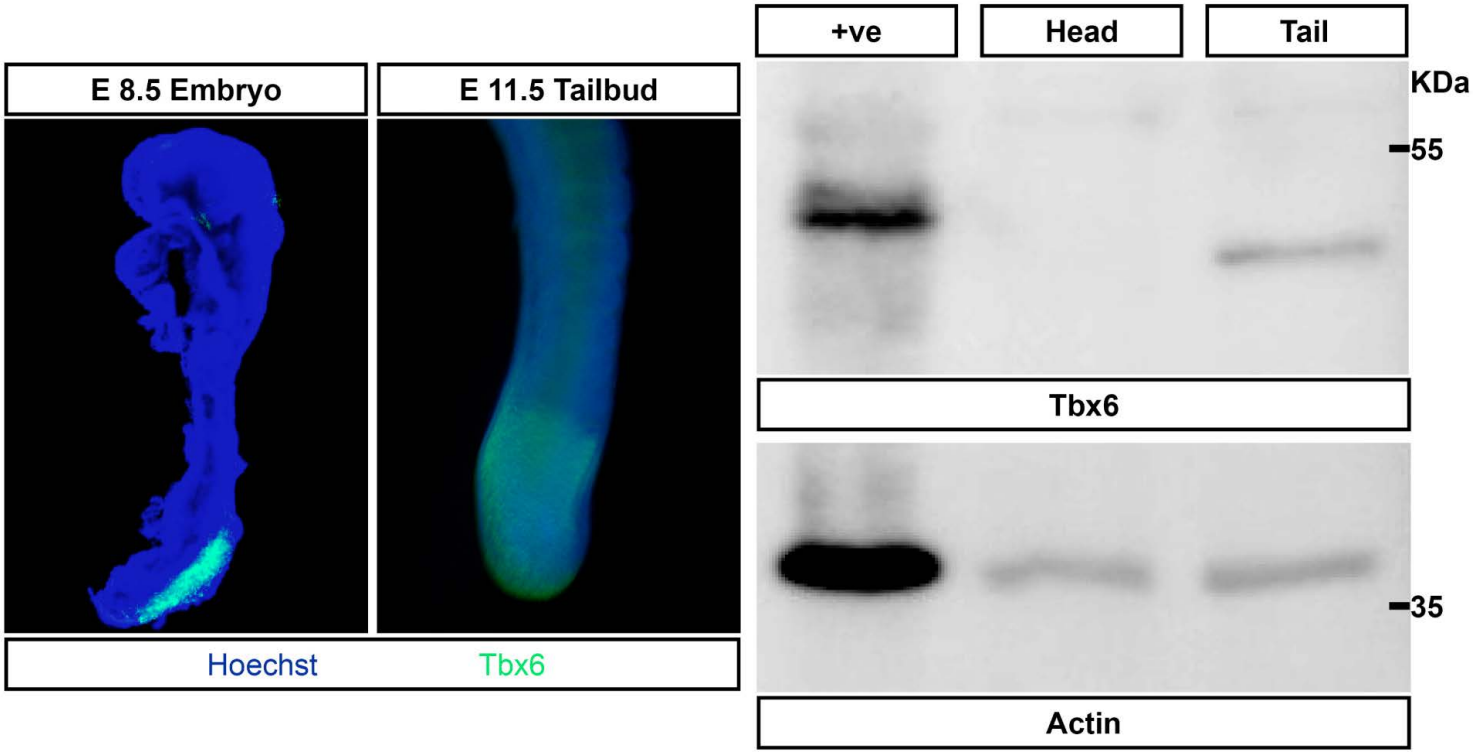

Figure S1. Specificity of the custom-generated antibody against Tbx6. Wholemount immunostaining assay shows staining in the presomitic mesoderm in the posterior end of E8.5 embryo and in the tailbud of E11 embryo; this attests to specific detection of Tbx6 by the antibody. In the immunoblot assay, the antibody detects a band below 55 KDa marker band. Head, embryonic tissue from interlimb level including head of E10.5 mouse embryos; Tail, embryonic tissue from hindlimb level including tail of E10.5 embryos; +ve, cell lysate from HEK culture overexpressing mouse Tbx6 cDNA as positive control. Actin is loading control. Absence of detection in the Head, while detection of a single band in the Tail shows specificity of the antibody.

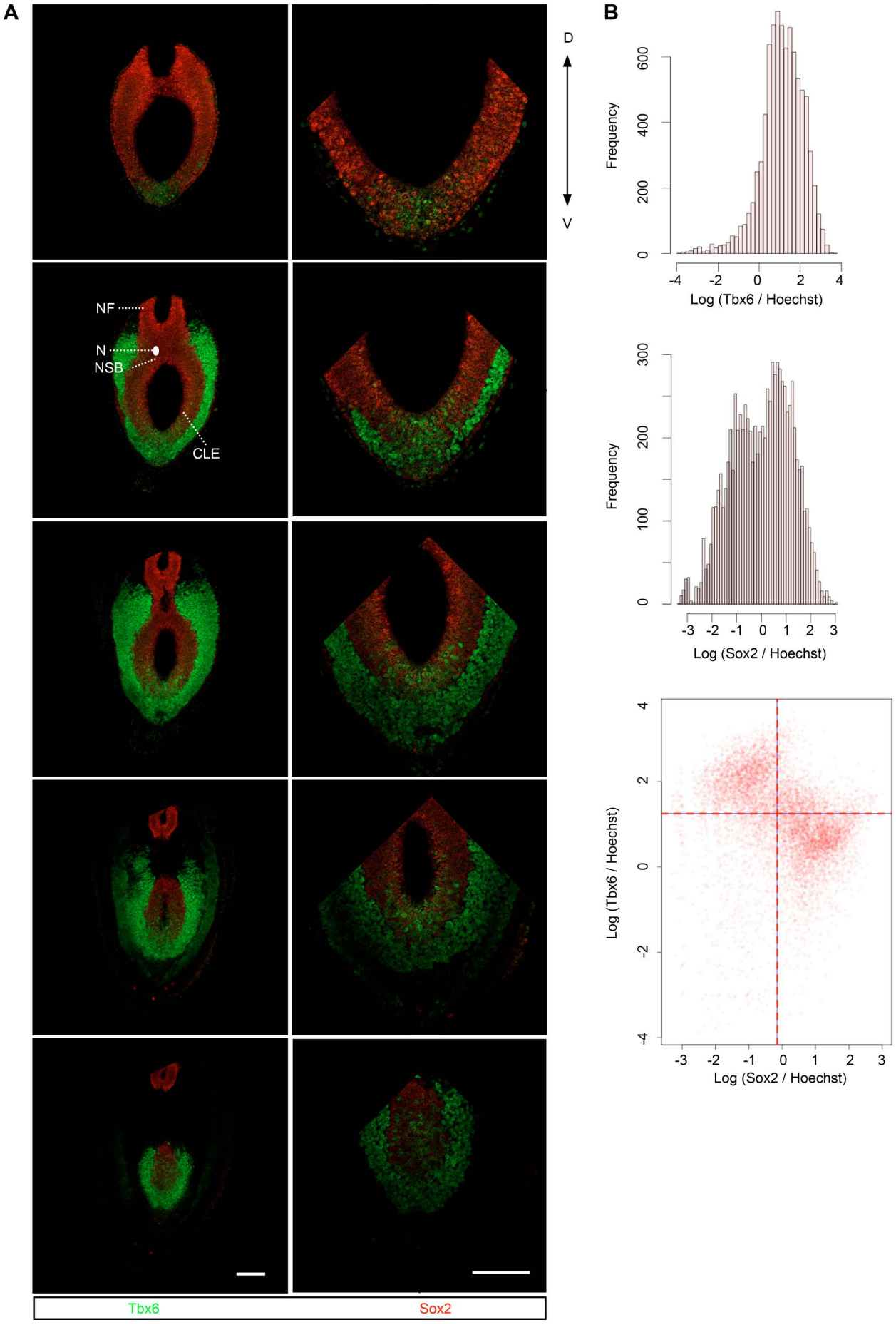

Figure S2. Tbx6 and Sox2 co-expression marks a new transient progenitor state of neuromesoderm lineage. A) Confocal optical section series from the posterior region of whole-mount immunostained E8.5 mouse embryo, starting from dorsal level at the top. Two different magnifications shown at comparable levels side-by-side. CLE, caudal lateral epiblast; N, Node; NF, neural fold; NSB, node-streak border; Scale bar, 100 μm. B) Quantitative image analysis of Tbx6 and Sox2 expression in the posterior region of immunostained E8.5 mouse embryo. The frequency of nuclei with a given relative fluorescence levels over Hoechst of Tbx6 and Sox2 are plotted. Scatter plot of Tbx6 against Sox2 identified two major cell populations, which expressed exclusively Tbx6 and Sox2. The plot shows how the thresholding was done. The threshold of Tbx6 levels were fixed at 1.25, i.e., fluorescence value above 1.25 was considered positive. For Sox2, threshold was at -0.15. We visually verified thresholding with the help of Tbx6 negative and Sox2 negative regions within the samples analyzed.

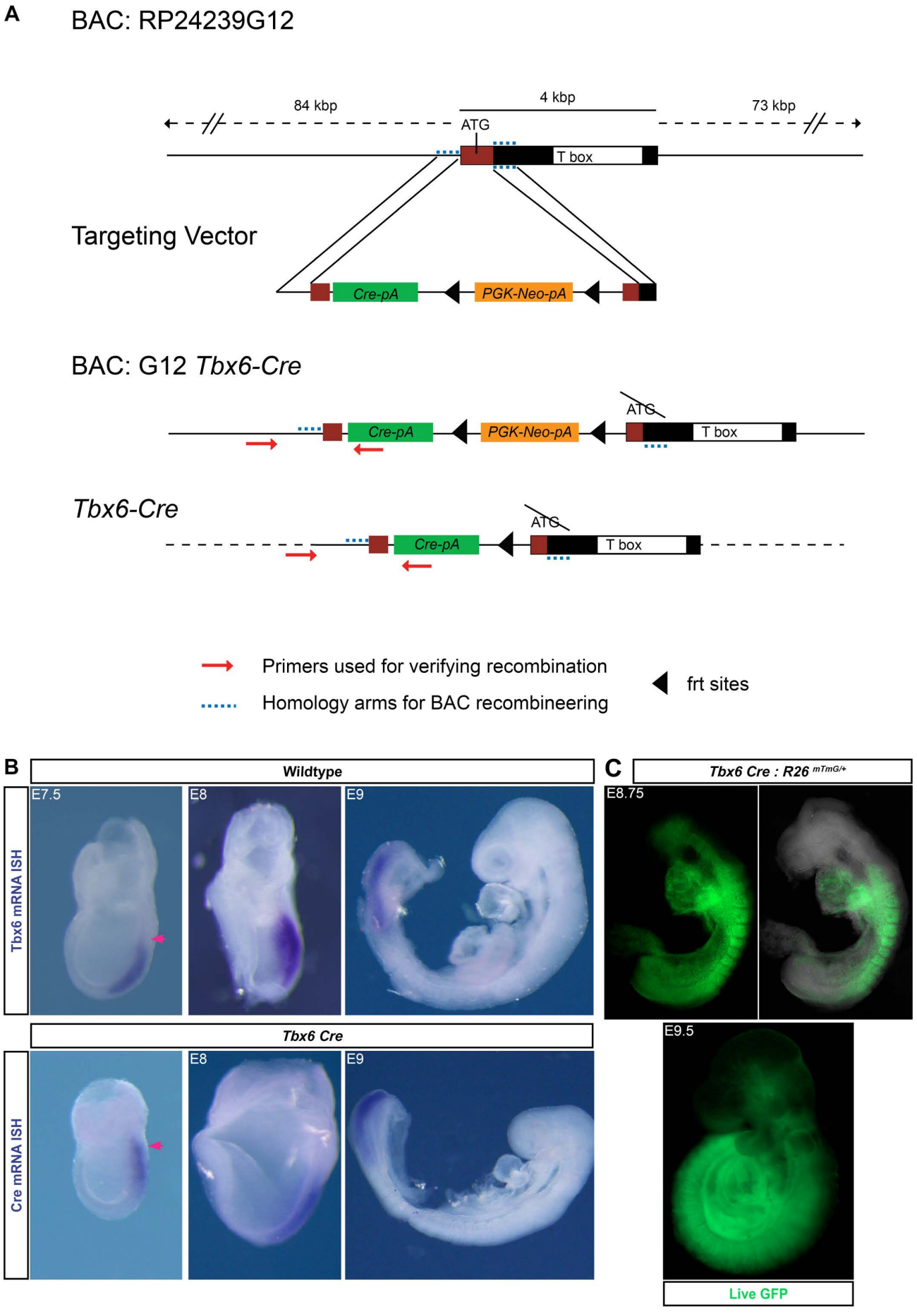

Figure S3. Transgene expression from *Tbx6-Cre* line recapitulates endogenous *Tbx6* expression. A) Schematic of the bacterial artificial chromosome (BAC) construct used to generate the *Tbx6-Cre* transgenic mouse line. See Supplementary Methods for details. B) Whole mount RNA in situ hybridization shows that *Cre* expression matches that of endogenous *Tbx6* transcript expression. Notable exception is the proximal posterior primitive streak region (pink arrows) at E7.5. The reporter expression is otherwise faithful to the endogenous gene expression. B) *Tbx6-Cre* mediated live GFP reporter expression marks *Tbx6* lineage in mesoderm and endoderm. C) Embryos imaged for live GFP expression. *Tbx6-Cre* lineage tracing shows broad reporter expression in mesoderm derivatives throughout the embryo in E8.75 and E9.5 embryos.

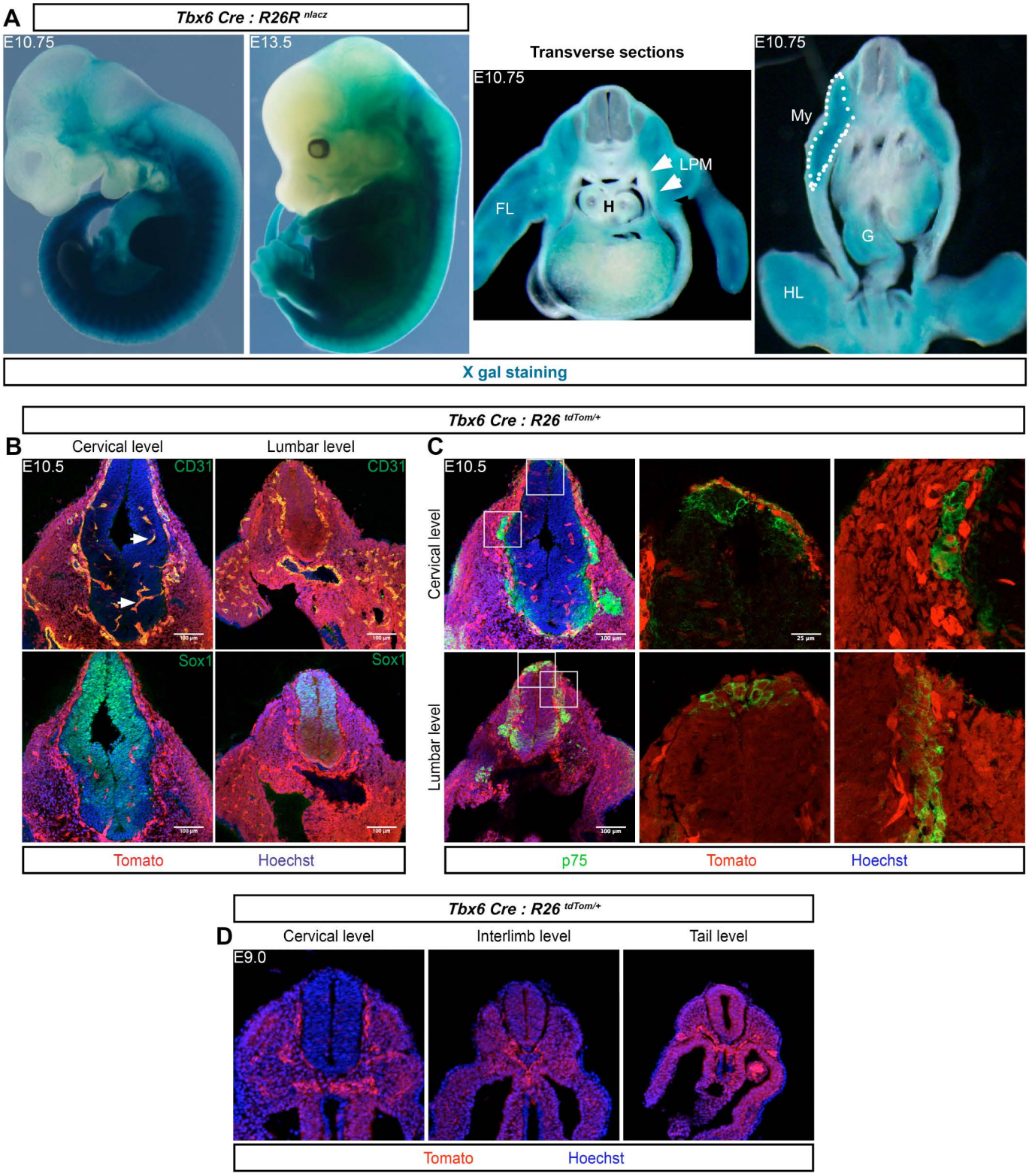

Figure S4. *Tbx6-Cre* reporter marks all mesoderm, endoderm as well as neural crest. A) Wholemount X-gal stained embryos show expression of the *Tbx6* lineage reporter in mesoderm derivatives throughout the embryo. Transverse vibratome sections of the X-gal stained embryos. The reporter expression in the myotome (My, outlined) of the somites, lateral plate mesoderm (LPM) as well as gut (G) shows appropriate expression of the reporter. FL, forelimb; HL, hindlimb;

H, heart. Note, the endodermal compartments (mid gut shown) are also marked by history of *Tbx6* expression. This is not surprising as Tbx6+ cells that ingress through the anterior primitive streak, where *Tbx6* is expressed, are mesendodermal cells, i.e., a population generating both mesoderm and endoderm. Reporter positive cells were observed in the developing heart and the mesodermal core of the pharyngeal arches. B) Immunostained cryosections show Tomato fluorescence and CD31 staining. Coexpression of CD31 with the Tomato (white arrows) shows that the lineage reporter positive cells in the neural tube at otic placode level are mesoderm-derived endothelial cells. At this level, no contribution is observed to neural progenitors. Coexpression of Tomato with Sox1 marks reporter expression in the neurepithelium. Reporter positive neural progenitors are observed from cervical level. C) Neuromesoderm contributes to neural crest. Neural crest emerges from neural plate border i.e., from the border between neural plate and surface ectoderm. Immunostaining with p75, a neural crest marker, shows limited contribution at cervical level and higher contribution at lumbar level. Note, grafting experiments have reported rare contribution of NMPs to neural crest (Wymeersch et al., 2016). Lineage tracing using a NMP marker Nkx1.2 also suggests NMP contribution to neural crest (Rodrigo Albors et al., 2016). Neural crest derives from the border of neural plate and surface ectoderm and contribute to peripheral nervous system as well as melanocytes. Therefore, contribution of NMP to crest would imply a much broader role for NMPs in the elongating body of vertebrates. All scale bars 100 μm. Scale bar for 4 images on right in C, 25 μm. D) Cryosections counterstained with Hoecsht show fewer reporter positive cells at cervical level with increasing numbers caudally. This data at E9 is consistent with E10.5 data shown in Fig. 3.

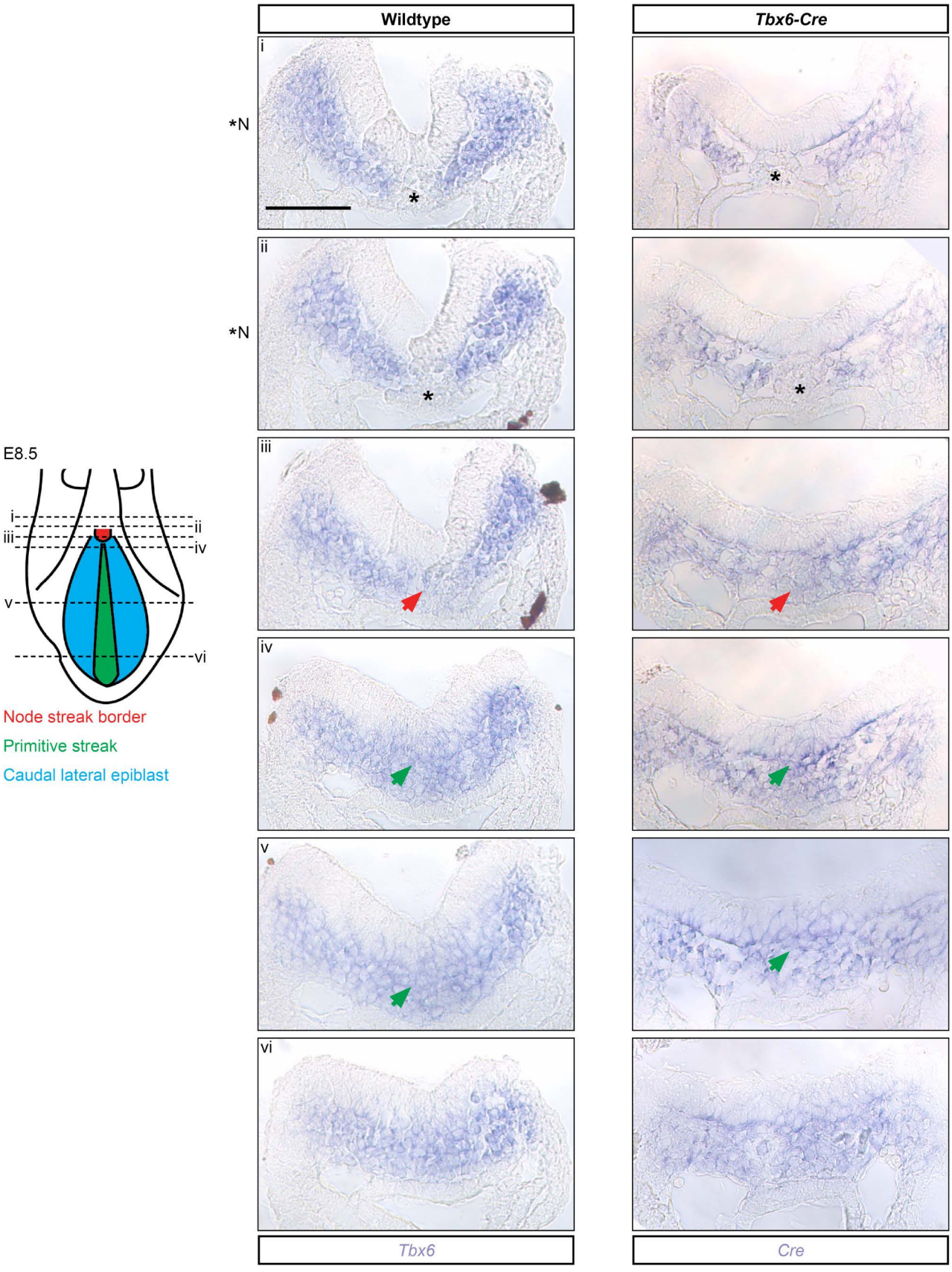

Figure S5. *Cre* transgene is expressed in NSB unlike that of endogenous *Tbx6*. Sections (10 μm thick) of paraffin-embedded embryos following wholemount RNA *in situ* hybridization. Scale bar 50 μm.

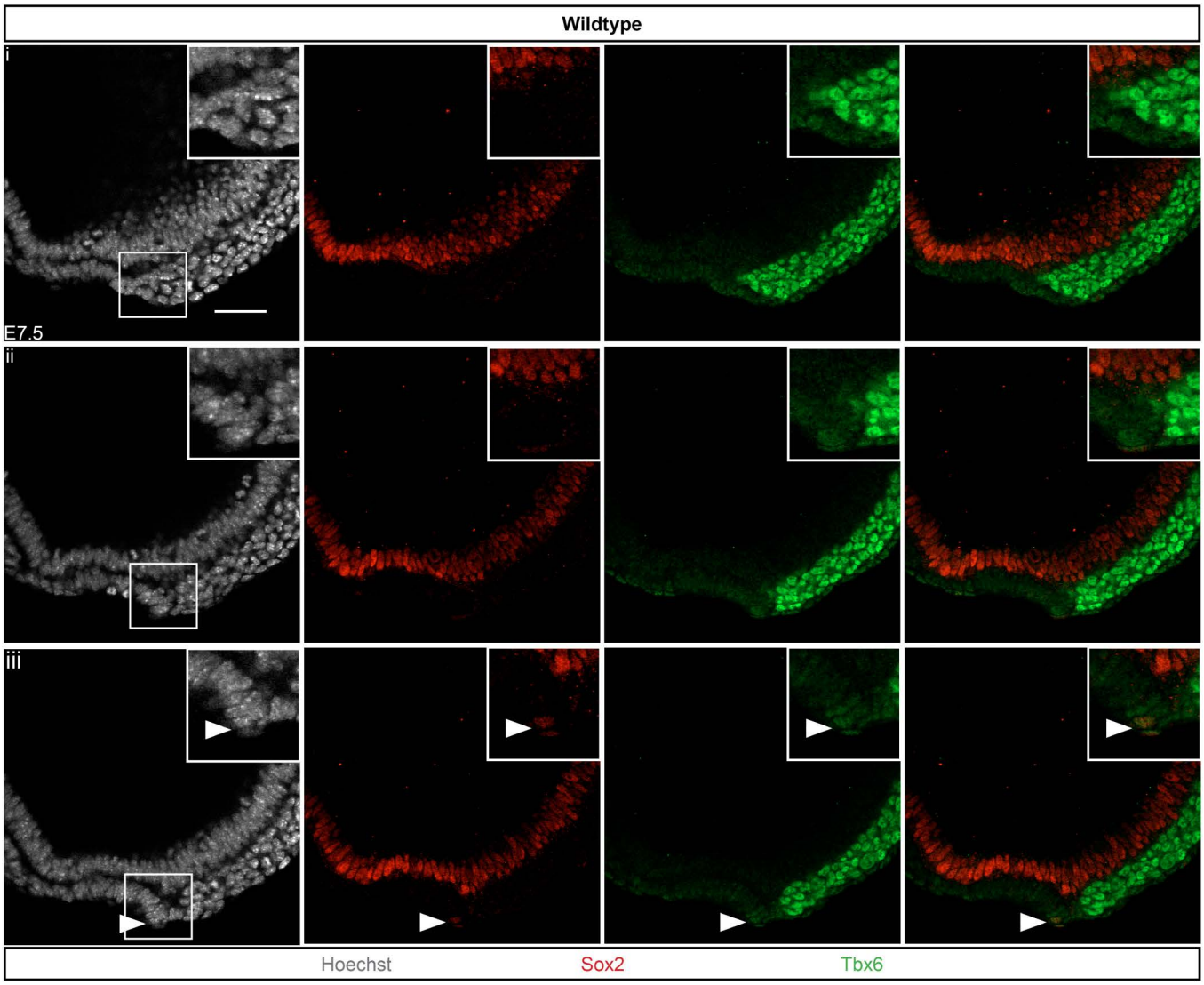

Figure S6. Tbx6+Sox2+ cells in NSB of E7.5 mouse embryos indicate early transient induction of *Tbx6* in NMP lineage. Sagittal confocal optical section series of mouse embryo stained against Tbx6 and Sox2. Scale bar 50 μm.

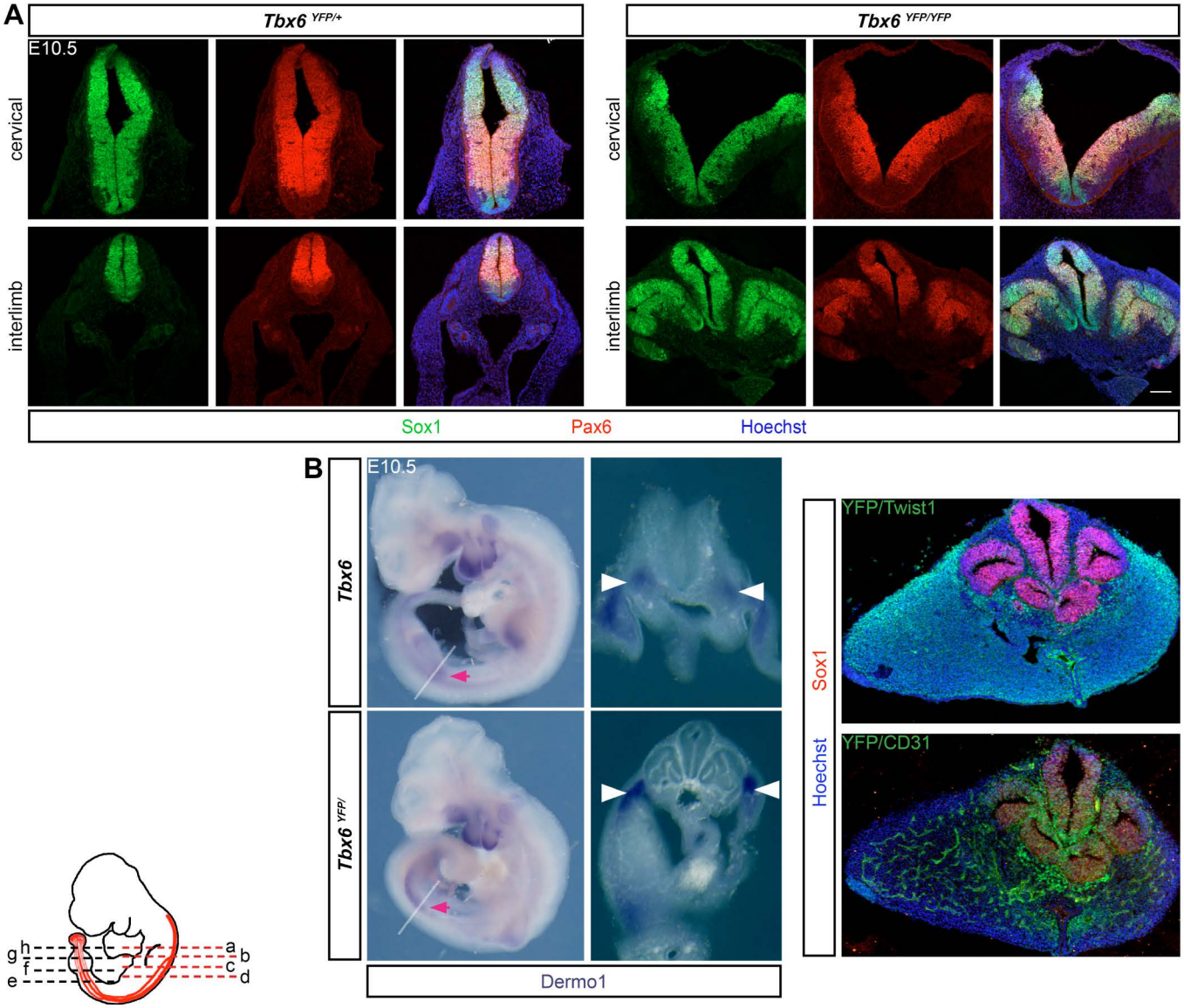

Figure S7. Ectopic neural tubes in *Tbx6* mutants. A) Posterior neural tube development appears unaffected in Tbx6 mutant. Immunostaining for Pax6 and Sox1 shows appropriate expression pattern of these markers and hence, no overt phenotype in posterior neural tube of *Tbx6* mutants. B) RNA in situ hybridization for Dermo1, wholemount and vibratome sections. Pink arrow points to lateral plate mesoderm in the hindlimb. The white line on the embryos indicates the plane and the location of the section shown on the left. White arrowheads indicate lateral plate mesoderm in the trunk. Immunostaining for Twist1 and CD31 (endothelial marker) reveal the presence and differentiation of posterior lateral plate mesoderm in the mutants at the hindlimb level. Residual YFP fluorescence in the green channel from $Tbx6^{YFP}$ allele is evident in CD31 image. These results show that the LMP develops as well as differentiates at the hindlimb level of the *Tbx6* mutants. LPM is generated by posterior primitive streak and is thought to have no contribution from NMPs. Nevertheless, the possibility of lateral plate mesoderm fate transformation as the cause for extra ectopic neural tubes at hindlimb level is formally ruled out by these experiments. Scale bar 100 μm. C) Vibratome sections reveal appearance of ectopic neural tubes at the axial level corresponding to the base of forelimb bud. Supernumerary ectopic tubes begin to form at the level in register with the top of the hindlimb bud. In this mutant, 5 ectopic neural tubes are seen. White arrowheads mark ectopic neural tubes.

Table S1: Anatomical distribution of Tbx6+Sox2+ transient progenitors in the CLE and primitive streak zone. Summary of the quantitative image analysis on the posterior part of CLE. The majority of cells are Sox2+ confirming that the analysis is primarily restricted to CLE/primitive streak zone. The fraction of Tbx6+ cells and hence, that of Tbx6+Sox2+ is likely an overestimate, since the images analyzed did not include Tbx6 negative NSB and anterior CLE. For reliable quantitative analysis, we chose to use high magnification images. At this magnification, the embryos were oriented such that the region of interest is optimally covered within the field-of-view. Note, the resultant diamond shape of the analyzed area includes a part of anterior streak as well. The inclusion of primitive streak would account for the Sox2 negative cells. Note, the mean distance from the midline for Tbx6+Sox2+ cells is less compared to that of uniquely Sox2+ cells. This indicates predominant distribution of the double positive cells in the medial compartment of CLE.

	Sox2			Tbx6			Double positive		
	Fraction %	Tip distance (μm)	Midline distance (μm)	Fraction %	Tip distance (μm)	Midline distance (μm)	Fraction %	Tip distance (μm)	Midline distance (μm)
Embryo 1	84.9	86	46.6	31.7	56	36.2	20.3	58.3	32.3
Embryo 2	86.7	111.7	43.4	41.5	97.5	40.1	31.7	106.9	37.9
Embryo 3	81	114.6	38.7	39.6	101.5	30.2	35	109	31.8
Mean	84.2	104.1	42.9	37.6	85	35.5	29	91.4	34
SD	2.91	15.74	3.97	5.2	25.19	4.99	7.71	28.68	3.39

Table S2: Details of antibodies used in the study. Custom generated antibody against Tbx6 was raised in rabbit. A peptide from murine Tbx6 with following sequence CFHGAPSHLPARTPSFAEAPDPGRPAPYS was used as immunogen.

Antibody	Company	Cat. Number	Dilution
CD31	BD biosciences	550274	1:100
Fn1	Millipore	AB2033	1:250
P75	Promega	G323A	1:500
Sox1	R&D	**AF3369**	1:100
Sox2	Santacruz	sc17320	1:100
Sox2 (used for co-staining with T)	Abcam	ab97959	1:500
T/Brachyury	Santacruz	B2605	1:250
Tbx6	Custom generated	-	1:250
Twist1	Abcam	ab50887	1:100

References:

Chapman, D. L., Agulnik, I., Hancock, S., Silver, L. M. and Papaioannou, V. E. (1996). Tbx6, a mouse T-Box gene implicated in paraxial mesoderm formation at gastrulation. *Dev Biol* **180**, 534–542.

Rodrigo Albors, A., Halley, P. A. and Storey, K. G. (2016). Fate mapping caudal lateral epiblast reveals continuous contribution to neural and mesodermal lineages and the origin of secondary neural tube. *bioRxiv* 45872.

Windner, S. E., Doris, R. a., Ferguson, C. M., Nelson, a. C., Valentin, G., Tan, H., Oates, a. C., Wardle, F. C. and Devoto, S. H. (2015). Tbx6, Mesp-b and Ripply1 regulate the onset of skeletal myogenesis in zebrafish. *Development* **142**, 1159–1168.

Wymeersch, F. J., Huang, Y., Blin, G., Cambray, N., Wilkie, R., Wong, F. C. K. and Wilson, V. (2016). Position-dependent plasticity of distinct progenitor types in the primitive streak. *Elife* **5**, 1–28.

Yasuhiko, Y., Haraguchi, S., Kitajima, S., Takahashi, Y., Kanno, J. and Saga, Y. (2006). Tbx6-mediated Notch signaling controls somite-specific Mesp2 expression. *Proc Natl Acad Sci U S A* **103**, 3651–3656.